Check for updates

Metal-catalyst-free growth of graphene on insulating substrates by ammonia-assisted microwave plasma-enhanced chemical vapor deposition

Shan Zheng, Guofang Zhong, [ID] * Xingyi Wu, [ID] Lorenzo D'Arsiè and John Robertson

We study the metal-catalyst-free growth of uniform and continuous graphene films on different insulating substrates by microwave plasma-enhanced chemical vapor deposition (PECVD) with a gas mixture of C_2H_2, NH_3, and H_2 at a relatively low temperature of 700–750 °C. Compared to growth using only C_2H_2 and H_2, the use of NH_3 during synthesis is found to be beneficial, in transforming vertical graphene nano-walls into a layer-by-layer film, reducing the density of defects, and improving the graphene quality. The effect of different insulating substrates (including Al_2O_3 and SiO_2) on the growth of graphene was studied under different growth temperatures, implying that the growth-temperature window and catalytic effect vary among insulators. The low activation energy barrier of Al_2O_3 proves it to be a more suitable substrate for the metal-catalyst-free growth of graphene at low temperature. These directly grown graphene films on insulators can be conveniently integrated into various electronic and optoelectronic applications avoiding any post-growth transfer processes.

1. Introduction

Graphene is a two-dimensional, single-layer sheet of sp^2-bonded carbon atoms packed into a honeycomb lattice. It has been regarded as one of the most attractive candidates for future electrical and optical applications owing to its excellent properties such as high carrier mobility, optical transparency, mechanical flexibility, and high thermal conductivity.[1,2] To fully realize its potential in real-world devices, metal-catalyst chemical vapor deposition (CVD) has been widely used in the large-scale, high-quality and cost-effective synthesis of graphene. However, this method has significant limitations in that the growth is normally carried out at ~1000 °C,[3–8] on a metal catalyst and requires a post-growth transfer process from metal onto an insulating substrate to make the device. The difficult transfer process usually results in polymer or metal residues, and wrinkling or breakage of graphene.[9–11] Therefore, it would be a great advantage to develop a direct, metal-free growth method of graphene onto insulating substrates at low temperature.

Unfortunately, insulating substrates generally display weak catalytic nature. The principle role of the catalyst in graphene growth is to dehydrogenate the precursor species[12] and to chemisorb the hydrocarbon as a mobile surface species to cluster into the growing graphene grains. Some oxides such as VO_x and Cr_2O_3 can act as dehydrogenation catalysts. The

stability of strongly bonded oxides such as ZrO_2 or HfO_2 against reduction by carbon and have been used to grow carbon nano structures.[13–16] There is also the novel idea of using remote copper or iron based catalysts which are then volatilized after the graphene growth.[17] Nevertheless, the direct growth of graphene onto insulating substrates has been frequently tried and tends to show degraded quality compared with those grown on metals.[18] In order to overcome the large energy barrier for graphene nucleation without metal catalysts,[19] even higher temperatures (1065–1650 °C) are required by thermal CVD to obtain graphene to compete with the metal-catalyzed growth.[20–24]

To lower the growth temperature, it is useful to consider plasma-enhanced chemical vapor deposition (PECVD).[25] The presence of energetic electrons, excited molecules/atoms, and free radicals generated in the plasma region can promote the decomposition of reactant gases, thus partly compensating for the weak catalytic nature of insulating substrates.[26] Several PECVD studies have been reported on SiO_2,[27–38] quartz,[27,31,38] glass,[34,39] and Al_2O_3[28,38] to explore the synthesis of graphene without metal catalysts at low temperature. Successful enlargement of isolated grain sizes has been realized using two-step growth in PECVD process.[27–30] However, extremely long growth times (over 9 hours)[27] or high-temperature pre-annealing (1000 °C)[29] was still needed to obtain isolated grains, and high mobility values were only measured on single grain devices due to discontinuous films.[28–30] Other groups tried to grow continuous graphene using PECVD. However, these

Department of Engineering, University of Cambridge, Cambridge CB2 1PZ, UK. E-mail: gz222@cam.ac.uk; Tel: +44 (0) 1223 748317

films suffered from common problems such as many defects, less surface uniformity,[31–39] and three-dimensional (3D) nano-wall growth.[31,34,37,40] All these drawbacks have limited graphene from fulfilling its excellent electrical properties and developing its advantage of atomic thickness. Therefore, a continuous, uniform, and two-dimensional graphene film with a low defect density is desirable, which can enable graphene integrated with the modern silicon electronics as well as other two-dimensional materials like transition metal dichalcogenides.

When it comes to device fabrication, insulators serve as gates in field-effect transistors (FETs), which have a strong influence on fulfilling the properties of graphene. However, the weak catalysis of insulators makes the selection of more proper insulating substrates essential in the metal-catalyst-free growth of graphene. SiO_2 might not be an ideal substrate for graphene FETs, because the high interface states density and impurity-induced trapped charges on SiO_2 substrates could cause carrier scattering issues that limit the performance of devices.[41] Recent studies suggest that using high dielectric constant (high-κ) materials like Al_2O_3 as gate insulators would boost the performance of devices due to the reduction of Coulomb scattering in graphene owing to the dielectric screening effect.[42] Therefore, the direct assembly of graphene on high-κ dielectrics would be useful. Atomic layer deposition (ALD) is a typical technique to obtain high-quality, thickness-controlled, pinhole-free high-κ thin films, which could provide a smooth and continuous surface for the graphene growth.[43] Furthermore, the graphene/high-κ dielectric structure could be easily applied onto any semiconductor or substrate for functional device fabrications. However, the only attempt of metal-catalyst-free PECVD growth of graphene on atomic layer deposited Al_2O_3 substrates[38] faced all the common problems mentioned above such as a high density of defects and multi-layer structures, but factors that degraded the quality and the mechanism behind it are not very clear.

Here, we demonstrate the metal-catalyst-free growth of graphene on SiO_2 and Al_2O_3 by PECVD to investigate the possible solutions to reduce the density of defects and 3D nano-walls. By decreasing the concentration of the carbon gas and especially introducing NH_3 in the growth, continuous and uniform graphene film with a low density of defects and no 3D nano-walls can be synthesized in our microwave PECVD system, thus the quality of graphene has been improved. Moreover, the graphene films produced on SiO_2 and Al_2O_3 under different growth temperatures have been compared, which can offer a better understanding of the weak catalytic effect of different insulating substrates on the graphene growth.

2. Experimental

The low-temperature growth of graphene on various insulators was carried out in a homemade microwave (2.45 GHz) PECVD system using reactant gases including C_2H_2, NH_3, and H_2, as schematically shown in Fig. 1a. Dielectric substrates were placed on a PBN/PG (Pyrolytic Boron Nitride/Pyrolytic Graphite) heater element enclosed in a metal cage with a honeycomb

mesh shield, as shown in the zoom-in image (Fig. 1b). This configuration can protect the samples from the ion-induced damage of the plasma ball, while the energetic and reactive species could pass through the mesh shield and reach the substrates to synthesize graphene. First, insulating substrates were heated to 650–750 °C after pumping down the chamber to 1×10^{-6} mbar. Second, H_2 was introduced at a rate of 400 sccm and a microwave plasma was ignited above the metal cage at a pressure of 15 mbar and a power of 600 W for 10 min. Third, C_2H_2, or C_2H_2 and NH_3 were added to the H_2 flow to start the graphene growth. The total gas flow rate was kept at 400 sccm (C_2H_2: 20–40 sccm, NH_3: 0–120 sccm, and H_2: 240–360 sccm). Finally, after three-hour growth, samples were cooled down by switching off the C_2H_2 and NH_3 flow, the plasma, and the heater power supply.

High-κ dielectric Al_2O_3 was deposited on SiO_2 (300 nm)/p-Si wafer via ALD. Before the ALD process, all the wafers were cleaned by sonication in acetone, isopropyl alcohol, and de-ionized water, and then dried with N_2. The cleaned wafers were placed in the chamber of Savannah S200 ALD reactor at the temperature of 200 °C with N_2 introduced as both carrier gas and purge gas. H_2O was used as the oxidant precursor, and trimethylaluminium (TMA) was the metal precursor for the deposition of Al_2O_3 dielectric surface. By changing the number of growth cycles, high-κ thin film was obtained with thicknesses of 3 nm measured by ellipsometry. Besides Al_2O_3, SiO_2 (300 nm)/p-Si substrates were used as the control group in the graphene growth. Other insulating substrates were also tested in our experiments to investigate the effect of insulating substrates on the graphene growth, including sapphire, quartz, MnO_2 spin coated on SiO_2 substrates, HfO_2 and TiO_2 deposited on SiO_2 substrates via ALD.

Several characterization techniques were used to investigate the quality and properties of the synthesized graphene. The surface morphology was observed by scanning electron microscopy (SEM, Carl Zeiss SIGMA, 1 kV), atomic force microscopy (AFM, Agilent 5500) and optical microscopy (Nikon ECLIPSE LV150N). The thicknesses of insulators were measured by ellipsometer (Gaertner L117). Raman spectroscopy (Renishaw InVia spectrometer, 457 nm excitation) was used to measure the crystallinity of graphene. Electrical properties were measured by a standard four-probe method (Keithley 4200-SCS Semiconductor Characterization System) at room temperature.

3. Results and discussion

We first tried to grow graphene by microwave PECVD using H_2 and C_2H_2. It is found that 3D graphene commonly appears on both SiO_2 and Al_2O_3 substrates at high C_2H_2 volume concentrations. However by decreasing the concentration of C_2H_2 from 10% to 5%, 3D nano-walls can be greatly reduced on both substrates as shown in the left column (the blue area) in Fig. 2. PECVD assisted growth of graphene can be regarded as the competing result of graphene nucleation and growth due to the saturation of hydrocarbon precursors and the etching of carbon by atomic hydrogen. The abundant carbon source results in repeated nucleation and vertical growth under an insufficient H_2
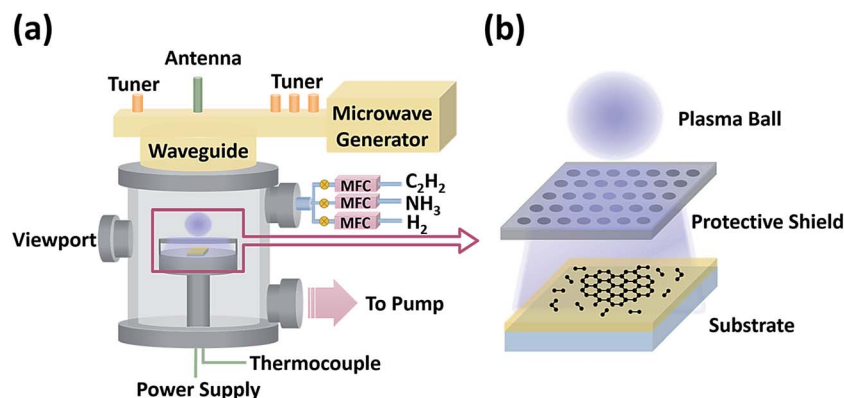
Fig. 1 Schematic illustrations of (a) the homemade microwave plasma-enhanced chemical vapor deposition system and (b) the zoom-in image of the graphene growth process.
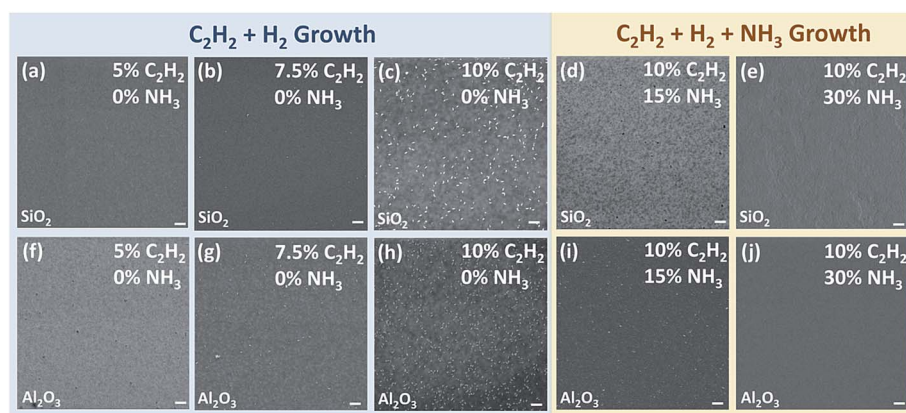

Fig. 2 SEM images of graphene grown directly on SiO_2 (a–e) and Al_2O_3 (f–j) at 750 °C for 3 hours by microwave PECVD using $C_2H_2 + H_2$ (left column) and $C_2H_2 + H_2 + NH_3$ (right column), respectively. The C_2H_2 and NH_3 concentrations are given in the images. The scale bars are 200 nm.

situation, which can be improved by reducing the concentration of carbon source to avoid excess carbon or increase the concentration of H_2 to gain a strong etching effect.[29,44,45] Compared with H_2 plasma, NH_3 plasma has been proved a more effective etching gas in generating atomic hydrogen species.[28,46–48] To investigate the effect of NH_3 on the growth of graphene, we intentionally keep the C_2H_2 concentration at a high level of 10%, which will lead to 3D nano-wall growth of graphene (Fig. 2c and h) using C_2H_2/H_2 plasma. With increasing NH_3 concentration from 0 to 30%, the surface morphology varies on both SiO_2 and Al_2O_3 substrates, as shown in the right column (the yellow area) in Fig. 2. By replacing 40 sccm H_2 with the same amount of NH_3 (15% NH_3), 3D nano-walls are reduced on both insulating substrates (Fig. 2d and i). By increasing the NH_3 concentration to 30%, layer-by-layer structures are obtained on both insulating substrates (Fig. 2e and j). For the SiO_2 substrate, the growth mode is in a layer-by-layer manner and the whole substrate is covered by graphene flakes. For the Al_2O_3 substrate, a continuous and uniform graphene sheet is directly synthesized on the substrate.

It has been also found that further increasing of NH_3 will lead to the growth of discontinuous graphene. Wei *et al.* studied

the growth of graphene by PECVD using only NH_3 and a carbon source such as C_2H_2, CH_4 or C_2H_4.[28] In their work, the growth temperature and the ratio of NH_3 and hydrocarbon gas were systematically varied to find the optimal growth condition. High-quality graphene with low density of defects has been synthesized using this binary growth. However, only discontinuous graphene domains were produced, which will limit its applications.

Fig. 3 is the corresponding Raman spectra of the as-grown samples shown in Fig. 2. The D peak, G peak, and 2D peak, centered at around 1370, 1580, and 2700 cm^{-1} respectively, are the predominant features in each Raman spectrum.[49] The 2D peak is a second-order two-phonon process related to a phonon near the K point in graphene, corresponds to the dispersive nature, and strongly depends on any perturbation to the electronic and/or phonon structure of graphene, therefore the 2D peak is regarded as the signature of graphene to differentiate itself from other sp^2 nanocarbons.[50] The G peak is caused by the stretching of the C–C bond in graphitic materials and is common in all sp^2 carbon system. The D peak is caused by the disorder in the sp^2 hybridized carbon atoms, and can be observed where symmetry is broken by edges or in samples with
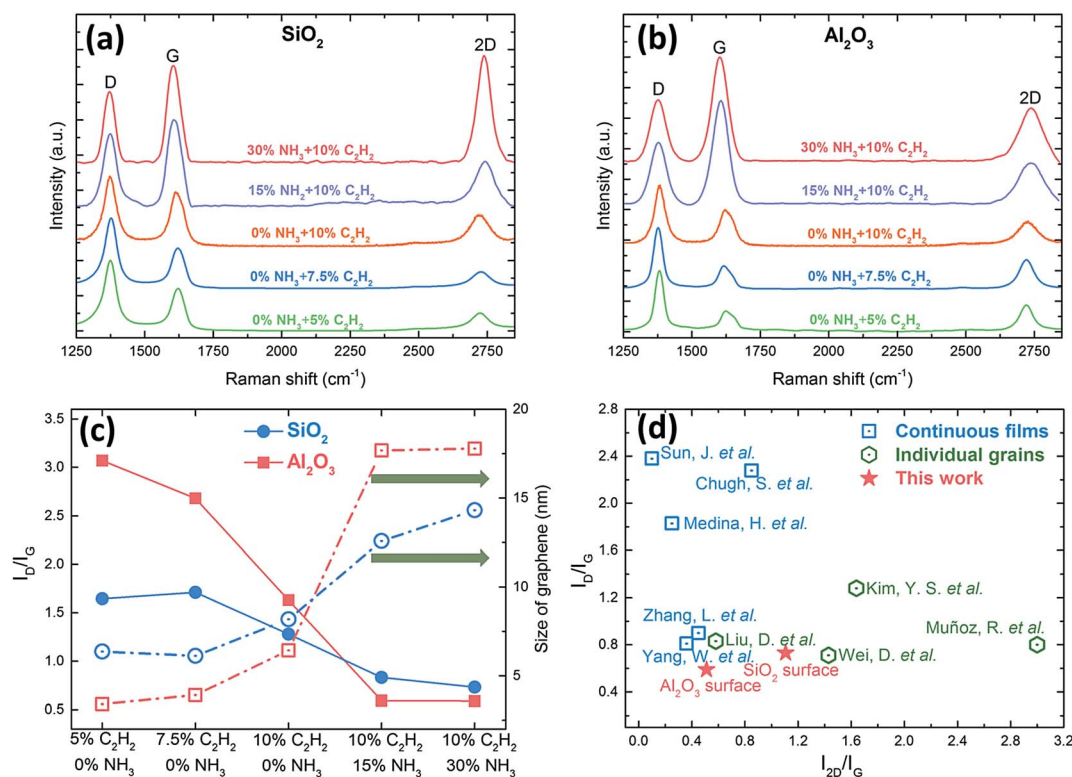
Fig. 3 (a, b) Corresponding Raman spectra of the as-grown samples shown in Fig. 2, and (c) the intensity ratios (I_D/I_G, solid symbols and lines) and the sizes of graphene (open symbols and dash dot lines) of the as-grown graphene films under different conditions for three-hour synthesis at 750 °C. (d) A summary of the intensity ratios of I_D/I_G and I_{2D}/I_G of synthesizing graphene on insulators by PECVD method. Blue square: continuous films (Sun, J. et al.,[32] Chugh, S. et al.,[31] Medina, H. et al.,[35] Zhang, L. et al.,[38] and Yang, W. et al.[36]); green hexagon: individual grains (Kim, Y. S. et al.,[33] Liu, D. et al.,[30] Muñoz, R. et al.,[27] and Wei, D. et al.[28]); red star: this work.

a high density of defects. In order to compare the intensities of G peaks and 2D peaks among different samples, all the D peaks in our Raman spectra were normalized.

The intensity ratio of D peak to G peak (I_D/I_G) can provide important information of the density of defects and the crystallite size of graphene.[51] When evaluating these two methods of reducing 3D nano-walls, the method of introducing NH$_3$ outweighs the method of decreasing the concentration of carbon source in reducing the density of defects and enlarging the crystallite size of graphene. Graphene grown on both SiO$_2$ and Al$_2$O$_3$ substrates using C$_2$H$_2$/H$_2$ plasma have a common feature that a relatively high density of defects caused by the high fraction of open edges of small crystallite sizes[51] (Fig. 3a and b). By introducing NH$_3$, I_D/I_G on both SiO$_2$ and Al$_2$O$_3$ substrates decreases greatly by 55.6% and 80.8% respectively (Fig. 3c). As I_D/I_G is inversely proportional to the grain size (L_a) for L_a above 2 nm, this can be used to study the level of disorder and assess the graphene quality. It can be also used to estimate the domain sizes (or crystal sizes) using Tuinstra and Koenig relation:

$$L_a \text{ (nm)} = C(\lambda_l)(I_D/I_G)^{-1}$$

where λ_l is the excitation laser wavelength, C (457 nm) $\sim$10.47 nm.[52,53] Fig. 3c also demonstrates the effect of reactant gases on L_a. It can be seen, L_a increases dramatically from

8.18 nm to 14.3 nm for graphene films grown on SiO$_2$ substrates and from 6.42 nm to 17.8 nm for Al$_2$O$_3$ substrates when increasing the NH$_3$ concentration from 0 to 30%.

The high sensitivity to the specific sp^2 nanocarbons makes the 2D Raman peak very useful in distinguishing graphene with different layers.[54] For metal-catalyzed CVD graphene, the intensity ratio of 2D peak to G peak (I_{2D}/I_G) $\approx$ 2 and a single Lorentzian 2D peak with a full width at half maximum (FWHM) of 30 cm^{-1} indicate monolayer graphene, the feature of $1 < I_{2D}/I_G < 2$ with the 2D peak being fitted to four Lorentzian peaks is for bilayer graphene, and the feature of $I_{2D}/I_G < 1$ with the 2D peak being fitted to two Lorentzian peaks suggests multilayer graphene.[3,4,55] However, for metal-catalyst-free CVD graphene, I_{2D}/I_G for monolayer graphene is lower (around 1.2–1.5) and the FWHM of 2D peak is broader (around 60 cm^{-1}) due to the non-negligible D peak resulting in the breakage of the hexagonal symmetry in graphene.[23,28,56] Among all the samples, the graphene grown on SiO$_2$ substrate under 30% NH$_3$ shows that $I_{2D}/I_G \sim 1.11$ and the FWHM of 2D peak $\sim$57.1 cm^{-1}, which implies monolayer graphene has been produced, and it further confirms the layer-by-layer structures observed by SEM in Fig. 2e. As for Al$_2$O$_3$, when increasing the NH$_3$ concentration from 15% to 30%, I_{2D}/I_G increases from 0.39 to 0.51, which suggests that the as-grown graphene is multilayer, but its layer number reduces with the increase of NH$_3$. Therefore, owing to the presence of NH$_3$, and the growth mode turns from vertical

graphene nano-walls to layer-by-layer films, and we can conclude that 30% NH_3 is the optical condition in our system to synthesize high-quality graphene with a lower density of defects, larger crystal sizes, and fewer layers for both substrates. Fig. 3d presents the summery of the intensity ratios (I_D/I_G and I_{2D}/I_G) of graphene synthesized on insulators by PECVD method below 900 °C. Compared to other published works, we have achieved the growth of uniform and continuous graphene films with the lowest I_D/I_G using $C_2H_2/(H_2 + NH_3)$ plasma, and Al_2O_3 demonstrates itself as a more competitive and suitable substrate for producing low-defect, large-area, and uniform graphene in comparison with SiO_2.

To determine the electrical properties of the synthesized graphene, we fabricated back-gate graphene FETs directly using the as-grown samples without any post-transfer process. By using electron-beam lithography, oxygen plasma etching, metal deposition (5 nm Cr/50 nm Au), and lift-off technology, numbers of graphene FETs can be fabricated each time other than a single graphene domain device reported in previous work.[28–30] The optical microscopy image of a typical graphene FET and its schematic structure are shown as the insets in Fig. 4a. Electrical characteristics were measured at room temperature in Keithley probe station. Fig. 4a shows the typical $I_{DS}–V_{DS}$ output curves of graphene devices fabricated from the sample of graphene prepared under 30% NH_3 (Fig. 2j) at various gate voltages (from −40 V to 40 V with a step of 20 V). The symmetrical linear behavior implies an ohmic contact between electrodes and graphene channel. The contact resistances are in the range of 3.8–6.6 kΩ $\square^{-1}$ measured by four-probe resistivity method. Fig. 4b gives the corresponding transfer curves (solid symbols) typical five graphene FETs. For comparison, Fig. 4b also plots the transfer curve (open cycles) of a FET prepared under only H_2 and C_2H_2. It can be seen that the FETs of graphene grown under 30% NH_3 show an ambipolar transfer characteristic with the Dirac point at negative gate voltages (−20 to −30 V). On the contrary, our FETs fabricated from graphene samples grown under C_2H_2/H_2 plasma do not show such an ambipolar transfer characteristic yet even though the gate voltage spans from −60 to +60 V. This indicates that the introduction of NH_3 has an n-type doping effect on the as-grown graphene, while the graphene is normally p-type FET behavior without NH_3. This is consistent with previous reports using NH_3 in the growth.[28,57] The average field-effect mobility was estimated to be around 16 cm^2 V^{-1} s^{-1}, and the mobility values were extracted from the slope of $I_{DS}–V_{BG}$ based on the constant capacitance model of parallel capacitors.[58]

The n-type doping of graphene can be also confirmed by Raman spectroscopy. Our Raman spectra in Fig. 3a and b show large downshifts of the G bands for samples prepared under different NH_3 concentrations (11.8–13.5 cm^{-1} for SiO_2 samples and 16.7–21.6 cm^{-1} for Al_2O_3 samples) compared with the sample without using NH_3. This is in accordance with reported N-doped graphene,[28,59] but different from ref. 60. Study has demonstrated that substitution of C atoms with graphitic N is n-type doping with a downshift in G band, while pyridinic and pyrrolic N is p-type doping with a upshift in G band.[61] This
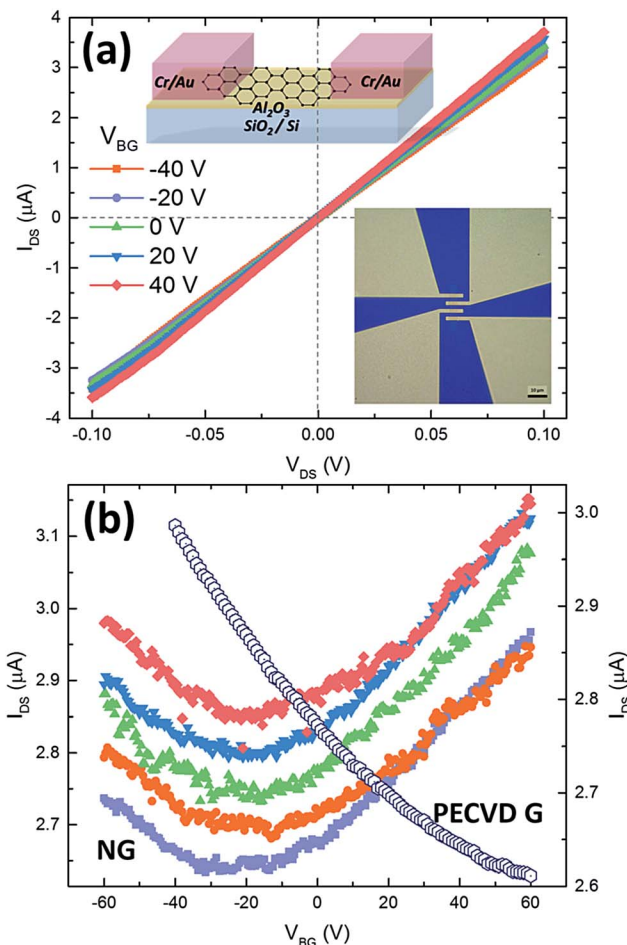

Fig. 4 Electrical properties of graphene synthesized directly on insulators. (a) Output characteristics of graphene FETs at different gate voltages. The inset is the schematic image of the device, and the optical microscopy image of the graphene device (the scale bar is 20 μm). (b) Transfer characteristics of five graphene FETs of N-doped graphene (NG, solid symbols) and a FET device of pristine graphene (PECVD G, open symbols) produced using only H_2 and C_2H_2 (V_{DS} at 100 mV).

means that our as-grown graphene is substitutionally doped by nitrogen atoms.

Besides the effect of NH_3 concentration on the growth, the SEM images also indicate insulators have an effect on the surface morphologies of graphene. Under the same NH_3 concentration and temperature, Al_2O_3 substrate favors a more effective nucleation stage and a faster growth stage compared with SiO_2, resulting in either a higher density of 3D graphene nano-walls (Fig. 2c and h) or a better coverage on the substrate (Fig. 2e and j). The reason seems to be the smaller activation barrier of Al_2O_3 in the graphene growth, and such a low energy barrier ensures the dissociative adsorption of C_2H_2 to carbon adatom could happen at low temperature.

To further confirm that, a controlled experiment was conducted on Al_2O_3 substrates under the same growth condition (40 sccm C_2H_2, 120 sccm NH_3, and 240 sccm H_2) by only decreasing the growth temperature from 750 °C to 650 °C. At
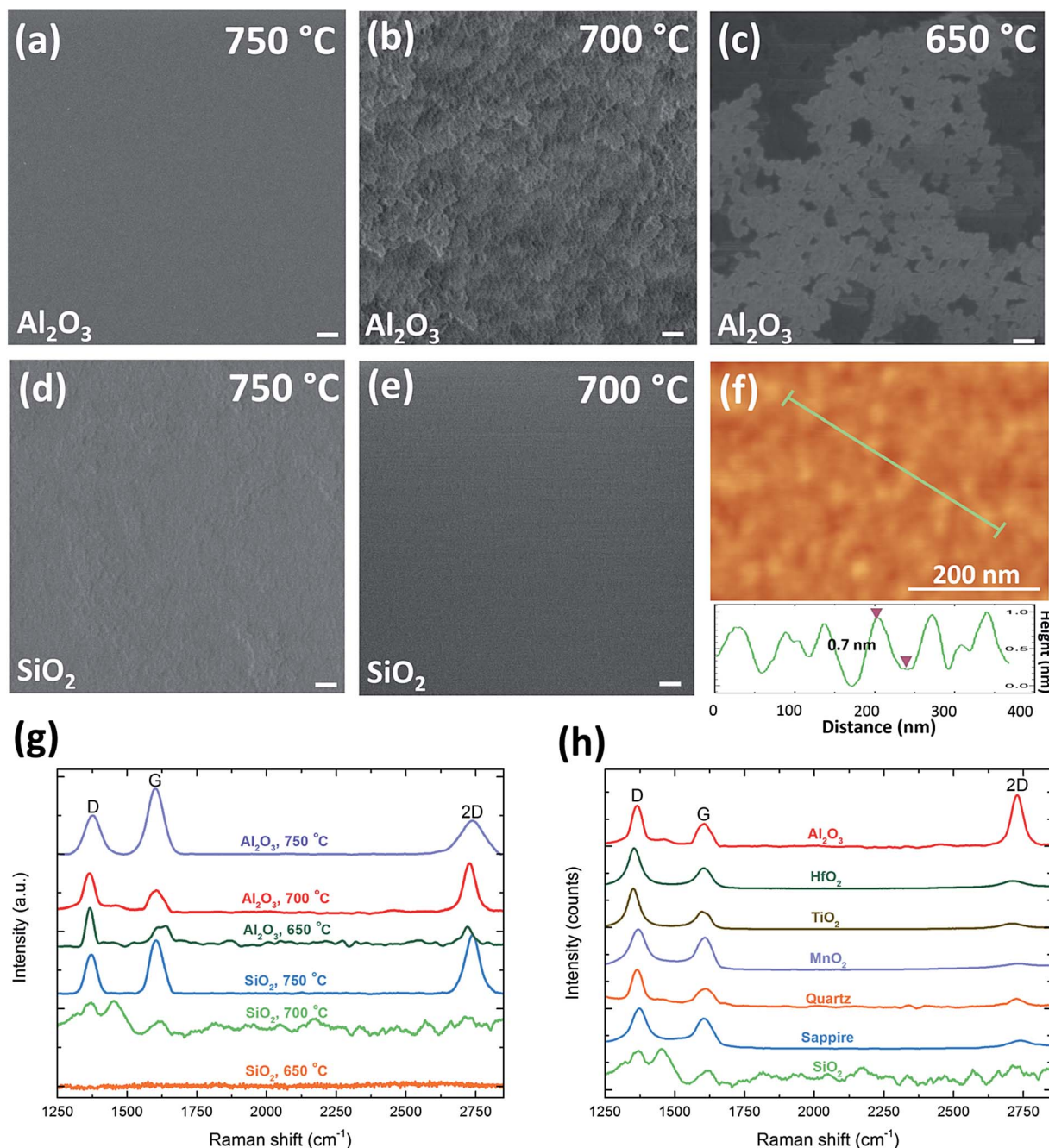
Fig. 5 Comparison of the growth under different temperatures with 30% NH_3 on Al_2O_3 substrates for 3 hours. SEM images of graphene grown at a temperature range of 750 °C to 650 °C on Al_2O_3 (a–c), and 750 °C to 700 °C on SiO_2 (d, e). The scale bars are 200 nm. (f) AFM image of sample (b) and the thickness of its graphene flakes. (g) Corresponding Raman spectra of graphene samples grown on both substrates in the temperature range of 650–750 °C. (h) Raman spectra of graphene sheets grown on different insulators with 30% NH_3 at 700 °C for 3 hours.

750 °C, a uniform and continuous graphene film is produced (Fig. 5a), and by decreasing the growth temperature to 700 °C, graphene flakes are generated on the whole Al_2O_3 substrate (Fig. 5b). The Raman spectrum of sample (b) shown in Fig. 5g presents a high level of defects ($I_D/I_G \sim 1.8$) due to the disorder and asymmetry of graphene caused by a large amount of domain boundaries and defects inside the nanographene. Although the density of defects is high, a sharp 2D peak ($I_{2D}/I_G \sim 2.27$ with the FWHM of 50.3 cm^{-1}) and the thickness of

0.7 nm measured by AFM (Fig. 5f) correspond to monolayer graphene. While at 750 °C, I_{2D}/I_G decreases to 0.51 and the 2D peak becomes broader, implying that bilayer or multilayer graphene prefers a higher temperature. By decreasing the temperature, the crystal size of graphene decreases with the maximum value of 17.8 nm obtained at 750 °C, implying that high temperature is beneficial to enlarge the size of graphene. When further decreasing the temperature into 650 °C, the whole substrate is partly covered with graphene flakes with a very high

density of defects, which indicates the temperature of 650 °C is not able to provide enough energy for the growth (Fig. 5c and g). Therefore, on Al_2O_3 substrates, monolayer graphene growth favors a lower temperature of 700 °C, while bilayer or multilayer graphene prefers a higher temperature of 750 °C, which can promote a uniform coverage of the whole substrate, alleviate defects and disorders, and enlarge the crystal size at the same time. More importantly, the morphology of graphene grown on Al_2O_3 at 700 °C has similar layer-by-layer structures as that grown on SiO_2 at 750 °C (Fig. 5d), while no graphene can be grown on SiO_2 substrates at a temperature below 700 °C (Fig. 5e), as confirmed by Raman spectra of SiO_2 in Fig. 5g. Therefore, the growth-temperature windows of these two insulators are different, which implies insulators might have different catalytic effect on the graphene growth. Part *et al.* carried out Density Functional Theory (DFT) calculations of activation barriers among Cu, Ni, and Al_2O_3 for graphene growth.[62] Among these activation barriers, the supply of C adatoms governed by E_{ad} and the enlargement of the graphene nuclei governed by E_{att} determine the lowest possible growth temperature.[62] From their theoretical calculations, both E_{ad} and E_{att} of Al_2O_3 are much lower than those of Cu while similar to the values of Ni. This indicates the graphene formation on Al_2O_3 could potentially be achieved at a temperature comparable to nearly the room-temperature synthesis of graphene on Ni.[63] Besides Al_2O_3 and SiO_2, other insulators including HfO_2, TiO_2, MnO_2, quartz, and sapphire have also been used as substrates under the same condition. As their Raman spectra with low 2D peaks and high D peaks show in Fig. 5h, they are not as suitable as Al_2O_3 to produce monolayer and low-defect graphene at 700 °C. Therefore, the similarity and difference in the morphology of graphene on various insulators suggest that insulators might have different growth windows due to their different activation barriers, and our experiments demonstrate that Al_2O_3 substrates have the lowest activation barrier among others, which enables it to produce the similar structures at relatively low temperature. Further theoretical studies *via* DFT simulations to calculate the activation barriers of various insulators are still needed in the future, which will be beneficial to understand the potential of different insulating substrates for the low-temperature growth of graphene.

Why can the growth mode of graphene be changed from 3D nano-walls to layer-to-layer films, and why is it n-type doped? Previous studies have shown that NH_3 is a much stronger etchant than H_2 to produce atomic hydrogen under plasma conditions, which can selectively etch away the amorphous carbon on graphene and remove defects generated at the graphene edges, thus keeping the edges atomically smooth and active during the graphene crystal growth.[28,44,57] However, this could not well answer the questions. In fact, the reactions in the plasma is very complicated, which can hardly be explained by a few simple chemical reaction equations. It depends not only on the plasma type (for example, DC plasma, RF inductively coupled plasma (ICP), microwave plasma, *etc.*) and the plasma power, but also on the plasma gases and pressure. Mao *et al.* intensively investigated the plasma chemistry of different binary gas mixtures (CH_4/H_2, CH_4/NH_3, C_2H_2/H_2 and C_2H_2/NH_3) for the synthesis of carbon

nanotubes/nanofibers by ICP enhanced CVD.[64] It is found that tens of species will be formed in the plasma. Although the atomic hydrogen produced by CH_4/NH_3 plasma is significantly higher than that by CH_4/H_2 plasma at 1 torr or high pressure, the atomic hydrogen produced by C_2H_2/NH_3 plasma is similar to that by C_2H_2/H_2 plasma. The most fundamental thing is that long-chain hydrocarbons such as $C_{2n}H_2$ and $C_{2n}H_6$ (n up to 6) are formed and become important in the C_2H_2/H_2 plasma. On the contrary, the formation of these long-chain hydrocarbon is less important in the C_2H_2/NH_3 plasma. We speculate that some long-chain hydrocarbons under C_2H_2/H_2 plasma can deposit randomly onto the substrate and develop into 3D nano-walls. By introducing higher concentration of NH_3 the formation of long chain hydrocarbon is greatly suppressed, therefore the growth of 3D nano-walls is eliminated. We also believe the atomic hydrogen plays an important role in our system. This is because NH_3 can be thermally decomposed to enough atomic hydrogen on the surface of substrate at 650–750 °C.[65] While the thermal decomposition of H_2 can be ignored due to its high stability. This explains why the quality of graphene is improved by introducing NH_3. On the other hand, active HCN species can be also produced in the plasma, which can attach to the edge of graphene and form the substitutionally N-doped graphene. This results in amounts of graphitic N,[57] leading to a Dirac point shift at a negative gate voltage and the downshifts of the G peaks in Raman spectra.

4. Conclusions

In summary, we have demonstrated a microwave PECVD method of synthesizing graphene on both SiO_2 and Al_2O_3 substrates without using any metal catalysts. By introducing NH_3 to suppress the formation of long-chain hydrocarbon in the plasma and to enhance the etching effect, we have obtained uniform and continuous graphene films with the lowest density of defects among all the PECVD growth of graphene. Further investigation of the effect of insulating substrates on the growth shows that the growth-temperature window and catalytic effect are different for each insulator owing to the different activation barrier. Al_2O_3 seems to own a lower activation barrier, which makes it a promising candidate as the substrate for the metal-catalyst-free growth of graphene at low temperature. This direct assembly of graphene on high-κ Al_2O_3 thin films can be flexibly incorporated into electronic and optoelectronic devices without any post-growth transfer process. More improvements are still needed in largely increasing the grain size, further reducing the growth temperature, and better controlling the number of layers. We believe our work provides an important step towards large-scale, low-cost and high-quality synthesis of graphene on arbitrary substrates.

References

1 K. S. Novoselov, A. K. Geim, S. V. Morozov, D. Jiang, Y. Zhang, S. V. Dubonos, I. V. Grigorieva and A. A. Firsov, *Science*, 2004, **306**, 666–669.

2 K. S. Novoselov, V. I. Fal'ko, L. Colombo, P. R. Gellert, M. G. Schwab and K. Kim, *Nature*, 2012, **490**, 192–200.

3 K. S. Kim, Y. Zhao, H. Jang, S. Y. Lee, J. M. Kim, K. S. Kim, J.-H. Ahn, P. Kim, J.-Y. Choi and B. H. Hong, *Nature*, 2009, **457**, 706–710.

4 X. Li, W. Cai, J. An, S. Kim, J. Nah, D. Yang, R. Piner, A. Velamakanni, I. Jung, E. Tutuc, S. K. Banerjee, L. Colombo and R. S. Ruoff, *Science*, 2009, **324**, 1312–1314.

5 Q. Yu, J. Lian, S. Siriponglert, H. Li, Y. P. Chen and S. S. Pei, *Appl. Phys. Lett.*, 2008, **93**, 113103.

6 P. R. Kidambi, C. Ducati, B. Dlubak, D. Gardiner, R. S. Weatherup, M. B. Martin, P. Seneor, H. Coles and S. Hofmann, *J. Phys. Chem. C*, 2012, **116**, 22492–22501.

7 R. S. Weatherup, B. C. Bayer, R. Blume, C. Ducati, C. Baehtz, R. Schlögl and S. Hofmann, *Nano Lett.*, 2011, **11**, 4154–4160.

8 G. Zhong, X. Wu, L. D'Arsie, K. B. K. Teo, N. L. Rupesinghe, A. Jouvray and J. Robertson, *Appl. Phys. Lett.*, 2016, **109**, 193103.

9 S. Bae, H. Kim, Y. Lee, X. Xu, J.-S. Park, Y. Zheng, J. Balakrishnan, T. Lei, H. R. Kim, Y. Il Song, Y.-J. Kim, K. S. Kim, B. Ozyilmaz, J.-H. Ahn, B. H. Hong and S. Iijima, *Nat. Nanotechnol.*, 2010, **5**, 574–578.

10 J. Kang, D. Shin, S. Bae and B. H. Hong, *Nanoscale*, 2012, **4**, 5527.

11 S. R. Na, J. W. Suk, L. Tao, D. Akinwande, R. S. Ruoff, R. Huang and K. M. Liechti, *ACS Nano*, 2015, **9**, 1325–1335.

12 W. Zhang, P. Wu, Z. Li and J. Yang, *J. Phys. Chem. C*, 2011, **115**, 17782–17787.

13 S. A. Steiner, T. F. Baumann, B. C. Bayer, R. Blume, M. A. Worsley, W. J. MoberlyChan, E. L. Shaw, R. Schlögl, A. J. Hart, S. Hofmann and B. L. Wardle, *J. Am. Chem. Soc.*, 2009, **131**, 12144–12154.

14 A. Kudo, S. A. Steiner, B. C. Bayer, P. R. Kidambi, S. Hofmann, M. S. Strano and B. L. Wardle, *J. Am. Chem. Soc.*, 2014, **136**, 17808–17817.

15 M. H. Rümmeli, A. Bachmatiuk, A. Scott, F. Börrnert, J. H. Warner, V. Hoffman, J. H. Lin, G. Cuniberti and B. Büchner, *ACS Nano*, 2010, **4**, 4206–4210.

16 A. Scott, A. Dianat, F. Börrnert, A. Bachmatiuk, S. Zhang, J. H. Warner, E. Borowiak-Paleń, M. Knupfer, B. Büchner, G. Cuniberti and M. H. Rümmeli, *Appl. Phys. Lett.*, 2011, **98**, 73110.

17 P.-Y. Teng, C.-C. Lu, K. Akiyama-Hasegawa, Y.-C. Lin, C.-H. Yeh, K. Suenaga and P.-W. Chiu, *Nano Lett.*, 2012, **12**, 1379–1384.

18 J. Sun, Y. Zhang and Z. Liu, *ChemNanoMat*, 2016, **2**, 9–18.

19 D. Geng, H. Wang and G. Yu, *Adv. Mater.*, 2015, **27**, 2821–2837.

20 J. Chen, Y. Wen, Y. Guo, B. Wu, L. Huang, Y. Xue, D. Geng, D. Wang, G. Yu and Y. Liu, *J. Am. Chem. Soc.*, 2011, **133**, 17548–17551.

21 J. Chen, Y. Guo, L. Jiang, Z. Xu, L. Huang, Y. Xue, D. Geng, B. Wu, W. Hu, G. Yu and Y. Liu, *Adv. Mater.*, 2014, **26**, 1348–1353.

22 Q. Liu, Y. Gong, T. Wang, W.-L. Chan and J. Wu, *Carbon*, 2016, **96**, 203–211.

23 M. A. Fanton, J. A. Robinson, C. Puls, Y. Liu, M. J. Hollander, B. E. Weiland, M. Labella, K. Trumbull, R. Kasarda, C. Howsare, J. Stitt and D. W. Snyder, *ACS Nano*, 2011, **5**, 8062–8069.

24 J. Hwang, M. Kim, D. Campbell, H. A. Alsalman, J. Y. Kwak, S. Shivaraman, A. R. Woll, A. K. Singh, R. G. Hennig, S. Gorantla, M. H. Rümmeli and M. G. Spencer, *ACS Nano*, 2013, **7**, 385–395.

25 J. Kim, M. Ishihara, Y. Koga, K. Tsugawa, M. Hasegawa and S. Iijima, *Appl. Phys. Lett.*, 2011, **98**, 91502.

26 X. Chen, B. Wu and Y. Liu, *Chem. Soc. Rev.*, 2016, **45**, 2057–2074.

27 R. Muñoz, C. Munuera, J. I. Martínez, J. Azpeitia, C. Gómez-Aleixandre and M. García-Hernández, *2D Mater.*, 2017, **4**, 15009.

28 D. Wei, L. Peng, M. Li, H. Mao, T. Niu, C. Han, C. Wei, W. Chen, A. Thye and S. Wee, *ACS Nano*, 2015, **1**, 1–15.

29 D. Wei, Y. Lu, C. Han, T. Niu, W. Chen and A. T. S. Wee, *Angew. Chem., Int. Ed.*, 2013, **52**, 14121–14126.

30 D. Liu, W. Yang, L. Zhang, J. Zhang, J. Meng, R. Yang, G. Zhang and D. Shi, *Carbon*, 2014, **72**, 387–392.

31 S. Chugh, R. Mehta, N. Lu, F. D. Dios, M. J. Kim and Z. Chen, *Carbon*, 2015, **93**, 393–399.

32 J. Sun, M. E. Schmidt, M. Muruganathan, H. M. H. Chong and H. Mizuta, *Nanoscale*, 2016, **8**, 6659–6665.

33 Y. S. Kim, K. Joo, S.-K. Jerng, J. H. Lee, E. Yoon and S.-H. Chun, *Nanoscale*, 2014, **6**, 10100–10105.

34 C. Yang, H. Bi, D. Wan, F. Huang, X. Xie and M. Jiang, *J. Mater. Chem. A*, 2013, 770–775.

35 H. Medina, Y.-C. Lin, C. Jin, C.-C. Lu, C.-H. Yeh, K.-P. Huang, K. Suenaga, J. Robertson and P.-W. Chiu, *Adv. Funct. Mater.*, 2012, **22**, 2123–2128.

36 W. Yang, C. He, L. Zhang, Y. Wang, Z. Shi, M. Cheng, G. Xie, D. Wang, R. Yang, D. Shi and G. Zhang, *Small*, 2012, **8**, 1429–1435.

37 A. Malesevic, R. Vitchev, K. Schouteden, A. Volodin, L. Zhang, G. Van Tendeloo, A. Vanhulsel and C. Van Haesendonck, *Nanotechnology*, 2008, **19**, 305604.

38 L. Zhang, Z. Shi, Y. Wang, R. Yang, D. Shi and G. Zhang, *Nano Res.*, 2010, **4**, 315–321.

39 J. Sun, Y. Chen, X. Cai, B. Ma, Z. Chen, M. K. Priydarshi, K. Chen and T. Gao, *Nano Res.*, 2015, **8**, 3496–3504.

40 A. T. H. Chuang, J. Robertson, B. O. Boskovic and K. K. K. Koziol, *Appl. Phys. Lett.*, 2007, **90**, 123107.

41 Y. Zhang, V. W. Brar, C. Girit, A. Zettl and M. F. Crommie, *Nat. Phys.*, 2009, **5**, 722–726.

42 S. Kim, J. Nah, I. Jo, D. Shahrjerdi, L. Colombo, Z. Yao, E. Tutuc and S. K. Banerjee, *Appl. Phys. Lett.*, 2009, **94**, 62107.

43 B. Dlubak, P. R. Kidambi, R. S. Weatherup, S. Hofmann and J. Robertson, *Appl. Phys. Lett.*, 2012, **100**(17), 173113.

44 L. Zhang, M. Ni, D. Liu, D. Shi and G. Zhang, *J. Phys. Chem. C*, 2012, **116**, 26929–26931.

45 L. Xie, L. Jiao and H. Dai, *J. Am. Chem. Soc.*, 2010, **132**, 14751–14753.

46 M. S. Bell, R. G. Lacerda, K. B. K. Teo, N. L. Rupesinghe, G. A. J. Amaratunga, W. I. Milne and M. Chhowalla, *Appl. Phys. Lett.*, 2004, **85**, 1137–1139.

47 M. S. Bell, K. B. K. Teo, R. G. Lacerda, W. I. Milne, D. B. Hash and M. Meyyappan, *Pure Appl. Chem.*, 2006, **78**, 1117–1125.

48 D. H. Lee, W. J. Lee and S. O. Kim, *Nano Lett.*, 2009, **9**, 1427–1432.

49 A. C. Ferrari, J. C. Meyer, V. Scardaci, C. Casiraghi, M. Lazzeri, F. Mauri, S. Piscanec, D. Jiang, K. S. Novoselov, S. Roth and a. K. Geim, *Phys. Rev. Lett.*, 2006, **97**, 187401.

50 M. S. Dresselhaus, A. Jorio, M. Hofmann, G. Dresselhaus and R. Saito, *Nano Lett.*, 2010, **10**, 751–758.

51 A. C. Ferrari, *Solid State Commun.*, 2007, **143**, 47–57.

52 A. C. Ferrari and J. Robertson, *Phys. Rev. B: Condens. Matter Mater. Phys.*, 2000, **61**, 14095–14107.

53 L. G. Cançado, K. Takai, T. Enoki, M. Endo, Y. a. Kim, H. Mizusaki, A. Jorio, L. N. Coelho, R. Magalhães-Paniago and M. a. Pimenta, *Appl. Phys. Lett.*, 2006, **88**, 12–14.

54 L. M. Malard, M. a. Pimenta, G. Dresselhaus and M. S. Dresselhaus, *Phys. Rep.*, 2009, **473**, 51–87.

55 D. Graf, F. Molitor, K. Ensslin, C. Stampfer, A. Jungen, C. Hierold and L. Wirtz, *Nano Lett.*, 2007, **7**, 238–242.

56 S. Xu, B. Man, S. Jiang, W. Yue, C. Yang, M. Liu, C. Chen and C. Zhang, *Nanotechnology*, 2014, **25**, 165702.

57 D. Wei, Y. Liu, Y. Wang, H. Zhang, L. Huang and G. Yu, *Nano Lett.*, 2009, **9**, 1752–1758.

58 D. K. Schroder, *Semiconductor Material and Device Characterization*, John Wiley & Sons, 2006.

59 L. Zhao, R. He, K. T. Rim, T. Schiros, K. S. Kim, H. Zhou, C. Gutierrez, S. P. Chockalingam, C. J. Arguello, L. Palova, D. Nordlund, M. S. Hybertsen, D. R. Reichman, T. F. Heinz, P. Kim, A. Pinczuk, G. W. Flynn and A. N. Pasupathy, *Science*, 2011, **333**, 999–1003.

60 S. M. Shinde, E. Kano, G. Kalita, M. Takeguchi, A. Hashimoto and M. Tanemura, *Carbon*, 2016, **96**, 448–453.

61 D. Deng, X. Pan, L. Yu, Y. Cui, Y. Jiang, J. Qi, W. X. Li, Q. Fu, X. Ma, Q. Xue, G. Sun and X. Bao, *Chem. Mater.*, 2011, **23**, 1188–1193.

62 J. Park, J. Lee, J.-H. Choi, D. K. Hwang and Y.-W. Song, *Sci. Rep.*, 2015, **5**, 11839.

63 J. Kwak, J. H. Chu, J.-K. Choi, S.-D. Park, H. Go, S. Y. Kim, K. Park, S.-D. Kim, Y.-W. Kim, E. Yoon, S. Kodambaka and S.-Y. Kwon, *Nat. Commun.*, 2012, **3**, 645.

64 M. Mao and A. Bogaerts, *J. Phys. D: Appl. Phys.*, 2010, **43**, 205201.

65 A. H. White and W. M. Melville, *J. Am. Chem. Soc.*, 1904, **27**, 373–386.